

Insight into the Interaction Mechanism of Nicotine, NNK, and NNN with Cytochrome P450 2A13 Based on Molecular Dynamics Simulation

Jorddy Neves Cruz,^{*,†,‡,§} Mozaniel Santana de Oliveira,[†] Sebastião Gomes Silva,[†] Antonio Pedro da Silva Souza Filho,[‡] Daniel Santiago Pereira,[‡] Anderson Henrique Lima e Lima,[§] and Eloisa Helena de Aguiar Andrade[†]

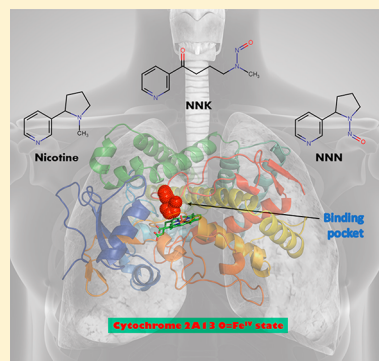
[†]Adolpho Ducke Laboratory, Emílio Goeldi Paraense Museum, Belém, Pará 66040-170, Brazil

[‡]Laboratory of Agro-Industry, Embrapa Eastern Amazon, Belém, Pará 66040-170, Brazil

[§]Laboratory of Planning and Development of Pharmaceuticals, Federal University of Pará, Belém, Pará 70770-901, Brazil

Supporting Information

ABSTRACT: Tobacco smoke contains various cancer-causing toxic substances, including nicotine and nitrosamines 4-(methylnitrosamino)-1-(3-pyridyl)-1-butanone (NNK) and *N'*-nitrosornicotine (NNN). The cytochrome 2A13 is involved in nicotine metabolism and in the activation of the pro-carcinogenic agents NNK and NNN, by means of α -hydroxylation reactions. Despite the significance of cytochrome 2A13 in the biotransformation of these molecules, its conformational mechanism and the molecular basis involved in the process are not fully understood. In this study, we used molecular dynamics and principal component analysis simulations for an in-depth analysis of the essential protein motions involved in the interaction of cytochrome 2A13 with its substrates. We also evaluated the interaction of these substrates with the amino acid residues in the binding pocket of cytochrome 2A13. Furthermore, we quantified the nature of these chemical interactions from free energy calculations using the Molecular Mechanics/Generalized Born Surface Area method. The ligands remained favorably oriented toward compound I (cytochrome P450 O=Fe^{IV} state), to undergo α -hydroxylation. The hydrogen bond with asparagine 297 was essential to maintaining the substrates in a favorable catalytic orientation. The plot of first principal motion vs second principal motion revealed that the enzyme's interaction with nicotine and NNK involved different conformational subgroups, whereas the conformational subgroups in the interaction with NNN are more similar. These results provide new mechanistic insights into the mode of interaction of the substrates with the active site of cytochrome 2A13, in the presence of compound I, which is essential for α -hydroxylation.



1. INTRODUCTION

Smoking is a worldwide public health problem, which causes addiction and involves several chemicals that cause diseases like chronic bronchitis, pulmonary emphysema, vascular diseases, and various types of cancer.^{1,2} The latest data from the World Health Organization show that the number of smoking-related deaths reached 7.2 million people per year and by 2030 may exceed 8 million deaths per year.³

Cigarette smoke contains various substances that are toxic to human health such as tar, benzene, formaldehyde, nitrosamines, etc.⁴ Tobacco-specific nitrosamines such as 4-(methylnitrosamino)-1-(3-pyridyl)-1-butanone (NNK) and *N'*-nitrosornicotine (NNN) become carcinogenic following metabolic activation by multiple cytochromes, which are enzymes capable of biotransforming a large number of substrates.^{5,6} In this biotransformation process, nicotine can give rise to NNK and NNN via nitrosation reactions.⁷

NNK and NNN undergo chemical reactions in the body, catalyzed by CYPs P450 2A6 and 2A13. CYP2A6 is mainly

located in the liver, whereas the 2A13 isoform is mainly found in the respiratory tract⁸ and has superior catalytic efficiency compared to CYP2A6,^{8,9} in metabolizing these compounds. CYP2A13 is also capable of metabolically activating nicotine.^{10,11}

CYPs P450 are able to catalyze various types of reactions.¹² Activation of nicotine, NNK, and NNN by CYP2A13 occurs via α -hydroxylation involving the participation of compound I (CYP450 O=Fe^{IV} state). Nicotine can undergo α -hydroxylation at the 2'- and 5'-carbon atoms^{11,13} while NNK undergoes α -hydroxylation at the 1'-carbon and *N*-methyl carbon. Products of these reactions form reactive metabolites capable of forming DNA adducts and causing chromosomal aberrations.^{14,15} NNN undergoes 2'-hydroxylation and 5'-

Special Issue: Molecular Simulation in Latin America: Coming of Age

Received: September 3, 2019

Published: October 17, 2019

hydroxylation (Figure S1), and its metabolites were shown to cause tumors in the respiratory tract and esophagus of rats and mice.^{16–18}

Recently, a number of theoretical studies using quantum mechanical methods such as density functional theory (DFT) and molecular dynamics hybrid simulations (quantum mechanics/molecular mechanics) have been published, where the fundamental reaction pathways and their stereoselectivity have been investigated in order to understand the mechanisms involved in the biotransformation of nicotine, NNK, and NNN by cytochrome P450s.^{17,19–26}

However, detailed information regarding essential protein motions, important for the understanding of the conformational mechanism of CYP2A13 and its biotransformation capacity, is not yet available. We also did not find any in-depth analysis of the molecular interaction between the pro-carcinogenic agent NNN with CYP2A13. DeVore and Scott used crystallography to probe the interactions between CYP2A13 and nicotine as well as NNK.²⁷ However, this analysis was performed in the presence of the heme group at the active site. In our study, we replaced heme with compound I, the catalytically active oxyferryl species essential for α -hydroxylation, catalyzed by CYP2A13. In our results, we refined the analysis of DeVore and Scott through optimization of receptor–ligand interactions, using molecular dynamics (MD) simulations. This allowed us to identify interactions not reported by the aforementioned authors.

Moreover, we utilized MD classic simulation and various methods of analysis to investigate the mode of interaction between CYP2A13 and nicotine, NNK, and NNN, for an in-depth understanding of the essential movements of the 2A13 isoform that are important to justify its biotransformation capacity. The MD simulations were performed with the Amber 16 package^{28–30} for a total time of 100 ns (ns) for each complex. We evaluated the convergence of the simulations using root-mean-square deviation (RMSD). We analyzed, in detail, the binding site of the enzyme and its interaction with the ligands. We also evaluated the importance of Asn257 in orienting the molecules in proper catalytic orientation, in addition to using principal component analysis (PCA) to identify the essential protein motions that are important for understanding the conformational mechanism of CYP2A13. Finally, we performed binding energy calculations with the Molecular Mechanics/Generalized Born Surface Area methods (MM-GBSA) to quantify the energy component values and the nature of the chemical interactions that favor the formation of the receptor–ligand complex.

2. MATERIALS AND METHODS

2.1. Molecular Docking. The molecular structure of NNN was designed using the GaussView 6 software³¹ and optimized with Gaussian 16³² using density functional theory, with the B3LYP/6-31G* basis sets.^{33,34} The NNN compound binding mode was proposed using Molegro Virtual Docker 5.5 software.^{35,36} The crystal structure of human cytochrome P450, isoform 2A13 complexed with nicotine (PDB ID: 4EJG),²⁷ was used as the target for NNN. We used this PDB ID as the receptor because NNN has a nicotine-like molecular structure and volume in the crystal. Therefore, the amino acids of the binding pocket are in a conformation suitable for NNN binding.

The MolDock Score (GRID) scoring function was used with a grid resolution of 0.30 Å and radius of 10 Å, encompassing

the entire connection cavity with its center at x , 22.56; y , –11.52; and z , 37.43. The MolDock SE algorithm was used with 50 runs, 3000 maximum interactions, and a maximum population size equal to 200. The maximum evaluation of 500 steps with a distance factor equal to 1 and an energy threshold of 100 was used in our protocol.

2.2. Preparation of Systems for MD Simulations. The crystal structure of CYP450 2A13 complexed with nicotine and NNK can be visualized in the PDB IDs 4EJG and 4EJH, respectively.²⁷ The initial structure for the CYP–NNN system was obtained from molecular docking methods, as described in the previous section.

The restrained electrostatic potential (RESP) protocol with the HF/6-31G* basis sets^{37,38} was applied to obtain the partial atomic charges of the atoms of each binder. The parameters of the ligand were constructed with the Antechamber module³⁹ using General Amber Force Field (GAFF).⁴⁰

All crystal structures of CYP450 2A13 found in the PDB were obtained with the heme group in the active site. However, the heme was replaced by compound I in our analysis, which is the catalytically active species critical for α -hydroxylation by CYP2A13. The force field parameters developed by Shahrokh and co-workers were used for compound I.⁴¹

The amino acid protonation state was characterized in neutral pH using the PDB 2PQR server.⁴² The systems were built with the tLEaP module of the Amber 16 package. The force field used to describe the protein in all simulations was ff14SB.⁴³ The protein–ligand system was solvated in an octahedron periodic box containing water molecules in the TIP3P model.⁴⁴ The partial charges were neutralized by adding chlorine counterions.

2.3. Setup of MD Simulations. The sander.MPI module of the Amber 16 package was used to perform energy minimizations. First, the water molecules and ions were optimized using 2000 cycles of steepest descent and 3000 cycles of the conjugate gradient. The position of receptor–ligand hydrogen atoms was then optimized using the 4000 steps of steepest descent algorithm and 3000 steps of the conjugate gradient. At the third stage, hydrogen atoms, water molecules, and ions were further optimized using the 2500 steps of steepest descent algorithm and 3500 steps of the conjugate gradient. Finally, all atoms were minimized using the 3000 steps of steepest descent algorithm and three steps of the conjugate gradient.

MD simulations were performed at a constant volume, by heating the systems up to 298 K. This heating was performed in five steps for a duration of 800 ps (ps). To restrict the atoms in the active site of the enzyme, a harmonic force constant of 25 kcal mol^{–1} Å^{–2} was applied, which was reduced by 5 kcal mol^{–1} Å^{–2} at each subsequent step. When the systems reached 298 K, another simulation was performed without any harmonic restriction for 250 ps. After all these steps, 100 ns production runs were performed for each complex established with CYP2A13.

The Particle Mesh Ewald method⁴⁵ was used for the calculation of the electrostatic interactions, and the bonds involving hydrogen atoms were restricted with the SHAKE algorithm.⁴⁶ The temperature control was performed with a Langevin thermostat⁴⁷ within a collision frequency of 2 ps^{–1}.

2.4. Principal Component Analysis (PCA). To analyze the conformational changes in CYP450 2A13 during its interaction with its ligands (nicotine, NNK, and NNN), we used the CPPTRAJ module⁴⁸ and the Amber 16 software to

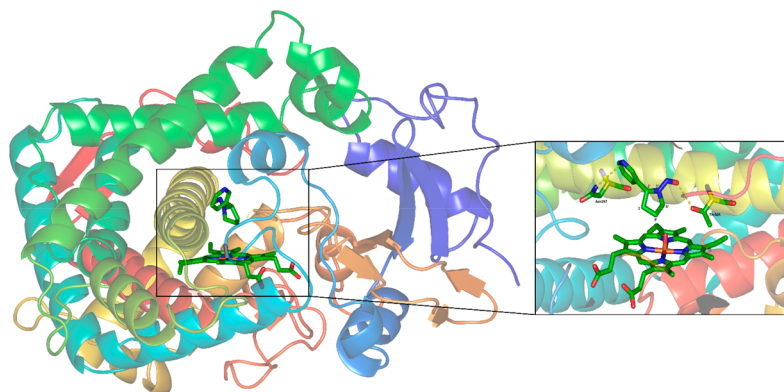


Figure 1. Molecular binding mode of NNN. Two residues (Asp297 and Thr305) are shown. Both established hydrogen bonds with NNN. Such residues are important for the permanency of the ligand in the binding pocket.

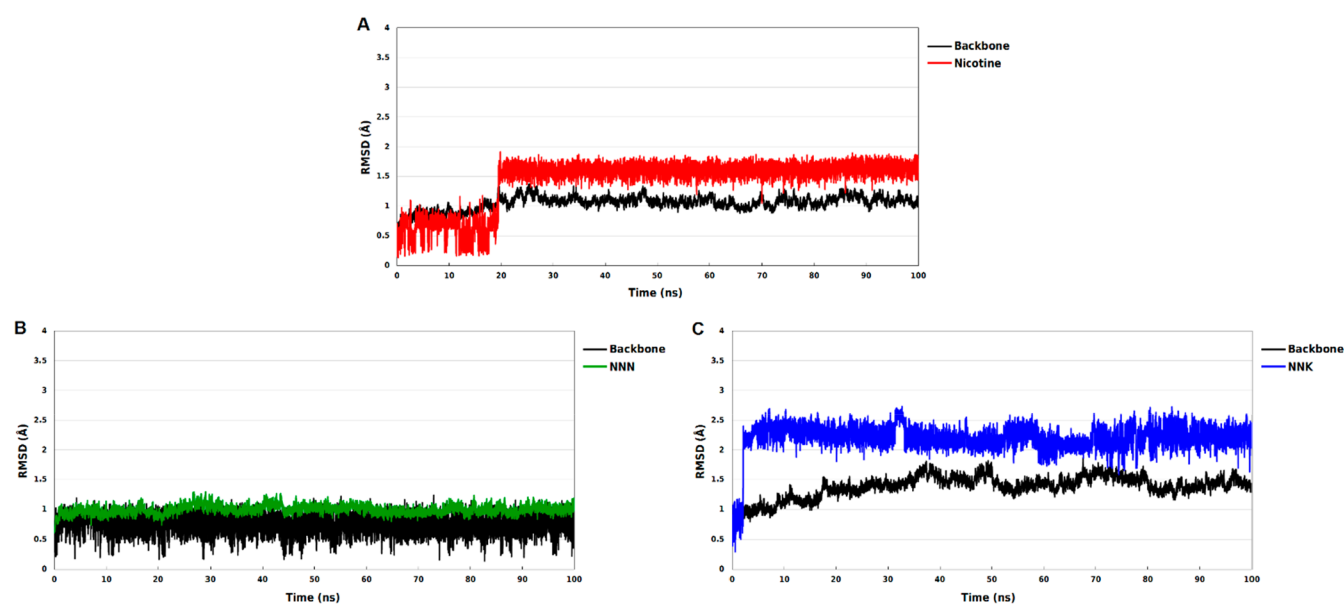


Figure 2. Time series of RMSD values for 100 ns of MD simulations. (A) Complex CYP–nicotine, (B) complex CYP–NNN, and (C) complex CYP–NNK.

run the PCA.^{49–51} The porcupine plot of protein motion was created using the Normal Mode Wizard (NMWiz)^{52,53} implemented in Visual Molecular Dynamics v1.9.3 (VMD).⁵⁴ Each frame of the trajectory was first adjusted by RMS-fit to a general mean structure to remove the global translational and rotational motion. The eigenvalues and eigenvectors were then obtained from the diagonalization of the covariance matrix of the $C\alpha$ atoms of the protein backbone. The amplitude of the motion is represented by the eigenvalues and the direction represented by the eigenvectors. The first major component (PC1) obtained is the one that represents the eigenvector with the greatest possible variation in the data set. The following eigenvectors (PC2, PC3, PC4, ..., PC n) represent a set of variations perpendicular to the previous main component. The movement of each main component was analyzed after projection of the coordinate of the MD trajectory.

2.5. Free Energy Calculations. To estimate the binding affinity (ΔG_{bind}) we used the Molecular Mechanics/Generalized Born Surface Area methods (MM-GBSA).^{55–57} The ΔG_{bind} was calculated according to the following equations:

$$\Delta G_{\text{bind}} = \Delta G_{\text{complex}} - \Delta G_{\text{receptor}} - \Delta G_{\text{ligand}} \quad (1)$$

$$\Delta G_{\text{bind}} = \Delta H - T\Delta S \approx \Delta E_{\text{MM}} + \Delta G_{\text{solv}} - T\Delta S \quad (2)$$

$$\Delta E_{\text{MM}} = \Delta E_{\text{internal}} + \Delta E_{\text{ele}} + \Delta E_{\text{vdW}} \quad (3)$$

$$\Delta G_{\text{solv}} = \Delta G_{\text{GB}} + \Delta G_{\text{NP}} \quad (4)$$

The free energy of bonding (ΔG_{bind}) is the summation of the interaction energy of the gas phase between protein–ligand (ΔE_{MM}), desolvation free energy (ΔG_{solv}), and system entropy ($-T\Delta S$). ΔE_{MM} is the result of the sum of internal energy ($\Delta E_{\text{internal}}$, sum of the energies of connection, angles, and dihedral), electrostatic contributions (ΔE_{ele}), and the van der Waals term (ΔE_{vdW}). ΔG_{solv} is the sum of the polar (ΔG_{GB}) and nonpolar (ΔG_{NP}) contributions. ΔG_{SA} was determined from the solvent accessible surface area (SASA) estimated by the linear combination of pairwise overlaps (LCPO) algorithm.

3. RESULTS

3.1. Binding Mode of the CYP2A13–NNN Complex. In order to develop the docking methodology, we first attempted

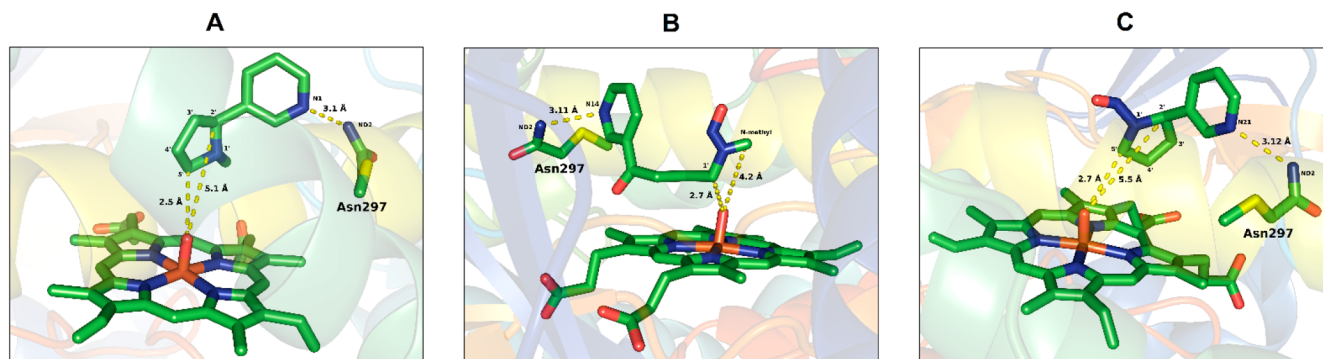


Figure 4. Average of the structure in the final 10 ns of simulation where the catalytic conformation of each ligand is displayed. The yellow lines demonstrate the distance between the O=Fe bond of compound I and the atoms undergoing hydroxylation. O=Fe abstracts the hydrogen from the carbon in the initial step in the hydroxylation process. The hydrogen atoms have not been shown in the images, for simplicity. (A) Complex CYP2A13–nicotine, (B) CYP2A13–NNK, and (C) CYP2A13–NNN.

with the heme in the binding pocket, while our MD simulations were performed in the presence of compound I, which is indispensable for the study of α -hydroxylation and the impact of these interactions on the structural architecture of cytochrome P450 2A13.

NNN underwent no large conformational variations as observed in its RMSD plot, which shows only small deviations. NNN retains the same binding mode to the docking structure, as to its initial structure probably because the molecular docking was carried out in the presence of compound I in the active site. Thus, the molecule conforms to the binding site. The same is not true for the CYP–nicotine complex, because the crystal structure of the complex was solved with heme at the site. Nicotine therefore underwent conformational change throughout the simulation to comfortably position itself to the binding site in the presence of compound I. NNN also established a hydrogen bond with a mean distance of 3.3 Å with Thr305. This interaction was essential in maintaining the binding conformation observed throughout the MD period.

NNK experienced a variation of approximately 1.25 Å in its RMSD plot at around 3 ns. This was due to a change in the nitrosamine moiety caused by steric hindrance from the O=Fe bond of compound I. After this movement, the ligand remained in equilibrium at the site, with no significant conformational changes in its binding mode.

3.2.2. Conformational Changes in the Enzyme Active Site.

In order to evaluate the conformational changes in the active site residues and in the ligands, we compared the structure corresponding to the last 10 ns of the simulation with the structure at the beginning of the simulations (crystal structure). The last 10 ns of the simulation present an MD trajectory with stable conformations. To obtain the average structure of the final 10 ns of MD simulations, we used CPPTRAJ. The representative structures were overlapped with the initial structures using PyMOL 2.3⁶¹ (Figure 3).

Nicotine was positioned closer to Asn297, with which it forms a hydrogen bond, critical for its activity.⁶² The remaining residues in the pocket underwent small conformational modifications. Nicotine may undergo hydroxylation at various sites of the methyl pyrrolidine ring. However, dominant hydroxylation occurs at the 5'-carbon.⁶³ The methylpyrrolidine ring remained directed toward the O=Fe bond of compound I, in an orientation favorable for hydroxylation. Cytochrome P450 is also capable of oxidizing the methyl radical of the pyrrolidine ring,⁶³ which was also observed in the MD

simulations, where the methyl radical was oriented toward compound I (Figure 3A).

NNK was positioned into the binding site with the surrounding residues adjusting to allow NNK to fit into the binding site properly. The pyrimidine ring of NNK was now more favorably oriented toward the Asn297 residue to establish a hydrogen bond interaction. Residues Phe209, Phe480, and Leu366 were repositioned from their initial conformations to allow the nitrosamine portion of the substrate to occupy a new space in the binding pocket. NNK can undergo α -methyl hydroxylation and α -methylene hydroxylation (1'-carbon).¹⁴ These atoms remained oriented toward compound I along the MD trajectory, exhibiting a catalytically favorable conformation (Figure 3B).

NNN underwent small conformational changes in its methyl pyrrolidine moiety that remained oriented toward compound I, and its pyridine ring underwent a small rotation, which allowed it to form a hydrogen bond with Asn297. NNN can undergo hydroxylation at the 2'- and 5'-carbon atoms to generate reactive metabolites that are eventually converted to DNA adducts, capable of inducing cancer in the respiratory tract.¹⁷ In our results, we observed that the nitrosopyrrolidine group remained in a favorable orientation to undergo hydroxylation (Figure 3C).

Xu and co-workers¹⁴ reported that the Phe cluster (Phe107, Phe111, and Phe209) constitutes a hydrophobic border for the interaction of CYP2A13 with NNK. In our MD simulations, we observed that these residues barring Phe209, also participated in the interaction with NNN and nicotine. van der Waals interactions occurred primarily with the side chain of the phenylalanine residues. Xu and co-workers¹⁴ also calculated the free energy decomposition and showed that the following residues are important for the interaction of CYP2A13 with NNK: Phe107, Phe111, Ala117, Phe118, Phe209, Asn297, and Leu370. These residues were also found to interact with nicotine and NNN, leading to the conclusion that these amino acids are important for the complex formation between CYP2A13 and its ligands.

3.3. Interaction within Residue Asn297 and the Catalytic Conformation. We investigated the hydrogen bonds (H-bonds) established between Asn297 and the substrates to verify their influence on the orientation of these molecules, in promoting a favorable catalytic conformation. Thus, we evaluated the bond length between the HD22 atom of Asn297 and the nitrogen of the pyridine ring of the ligands.

The schematic representation of the H-bonds formed, along with the mean distances between the hydroxyl-bearing carbons and O=Fe, are shown in Figure 4. Table 1 shows the mean distances and the lifetime of the H-bonds.

Table 1. Hydrogen Bonds Determined in the CYP2A13–Ligand Complex

acceptor	hydrogen donor ^a	average distance (Å)	occupancy (%) ^b
nicotine@N1	Asn297@ND2-HD22	3.10	91.26
NNK@N14	Asn297@ND2-HD22	3.11	85.81
NNN@N21	Asn297@ND2-HD22	3.12	84.25

^aThe hydrogen bonds were determined according to the condition of donor–acceptor atom distances being ≤ 3.5 Å and acceptor–donor hydrogen donor angle being $\geq 120^\circ$. ^bOccupancy is defined as the percentage of time that the hydrogen bond was formed during the 100 ns simulation time.

Schlicht and co-workers⁶⁴ reported that the N297A mutation impairs NNK and NNN metabolism, as this mutation causes the loss of an essential H-bond, which facilitates engagement of the target with the ligands in the active site. In order to evaluate the molecular impact of this mutation, the authors performed docking using CYP2A13 N297A in the presence of the heme group and not compound I, which participates in the α -hydroxylation reaction of these substrates. However, in our previous analyses, it was clear that compound I influenced the binding mode of the substrates, so it was more appropriate to analyze the H-bond in the presence of compound I at the binding site, as we have done. In addition, our H-bond analyses were performed on 100 ns MD trajectories, which allowed larger conformational samplings not possible in molecular docking analyses.

H-bonds formed between nicotine, NNK, and NNN had a time of approximately 91, 85, and 84 ns. The longest lasting H-bond was therefore recorded for nicotine. This demonstrates the great importance of this interaction in orienting this molecule in a favorable conformation for metabolic activation. Thus, the loss of this H-bond, caused by mutations at N297, may decrease nicotine metabolism as well as that of NNK and NNN, which are structurally similar to nicotine.

The results also showed the importance of the H-bond in the formation between Asn297 and the compounds NNK and NNN, demonstrating that this interaction in the complexes is significantly established.

3.4. Collective Motions Obtained by PCA. We used PCA to identify motion differences of CYP2A13. The projections of the conformational behaviors during the MD simulations, along the direction of the eigenvectors 1 and 2, can be observed in Figure 5.

The plots of eigenvectors 1 and 2 represent the essential movements of the protein that have been assembled into different conformational subgroups and are color coded along the MD trajectory.

Graphs A, B, and C show that there is a distinct separation between the dominant motions of the protein, but in chart C a greater similarity between the conformational subgroups assumed by the enzyme is observed.

The PC1 vs PC2 plot for all three complexes showed that the enzyme was able to explore different conformations when interacting with nicotine, NNK, and NNN. Thus, it is evident that CYP2A13 presents different conformational mechanisms along the trajectories to perform the α -hydroxylation of these substrates.

It is important to cite the difference between the conformations assumed by cytochrome P450, when interacting with nicotine, NNN, and structurally similar molecules, which have the same binding site and occupy a similar volume. When interacting with nicotine, the conformational subgroups of the enzyme are more diverse, whereas the conformations assumed by cytochrome when interacting with NNN are more similar to each other. This implies that the structural clusters of the protein are grouped within a common conformational subspace. This demonstrates that CYP2A13 exhibits great structural plasticity when interacting with substrates that are structurally similar.

3.5. Dominant Motions of the FG and BC Loops. In the CYP450 complex, the active site is buried in the enzyme, so that the substrate, products, gaseous molecules, and water can access the site, to form channels. The products are led out of the enzyme after the reaction, through different routes. The movements of the FG and BC loops are related to the formation of channels 2a, 2ac, 2c, and 2e, as per the nomenclature used by Cojocar and co-workers.⁶⁵ Thus, we investigated the dynamics of the FG and BC loops to evaluate their influence on the channels formed within the enzyme.

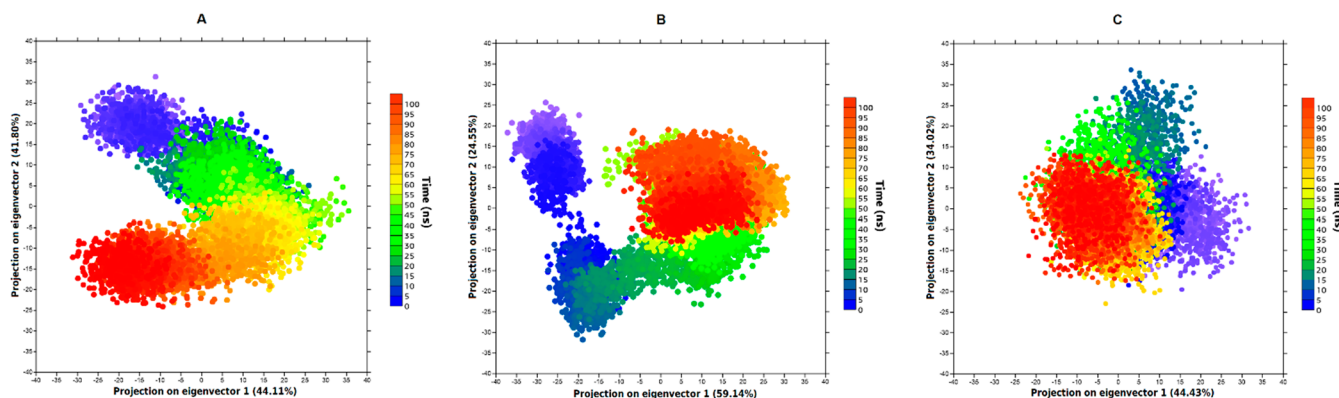


Figure 5. Projection of the first and second major components along the MD simulation trajectories for the complexes established by CYP2A13 with (A) nicotine, (B) NNK, and (C) NNN.

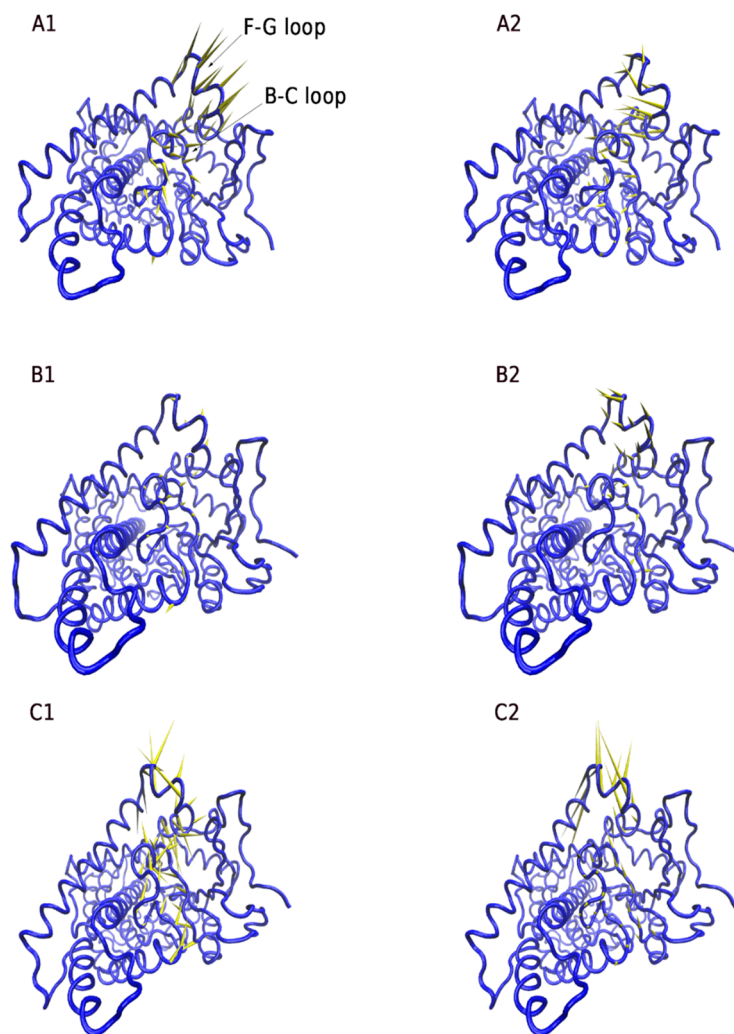


Figure 6. Representation of the dominant motions of the FG and BC loops obtained from PC1 and PC2 for the complexes established with (A) nicotine, (B) NNK, and (C) NNN.

To qualitatively represent and analyze the differences in the dominant motions in the FG and BC loops, we generated porcupine plots for the first and second eigenvectors of the MD trajectories (Figure 6).

The backbones have different directions and lengths, which indicate the tendency and amplitude of the movements. The analysis of PC1 and PC2 of nicotine shows that the FG and BC loop have synchronous opening and closing movements in similar proportions, since the lengths of the backbone observed in these projections are equivalent. Such coordinated movement may influence the opening and closing of the channels 2a and 2ac, which are situated at the top of the protein structure.

In the complex established with NNK, the FG and BC loops in PC1 showed almost no movement. In PC2, the FG loop presented a slight tendency of movement toward the binding site. The small amplitudes of movements in this system may be related to the greater number of residues with which the NKK is able to interact, thus restricting the possibility of greater movement of this loop. The low dynamics of movements in these loops suggest that the formation of the canals does not involve major conformational changes.⁶⁵

The BC loop in the CYP–NNN system presented a great change of movement in relation to the other complexes,

because in PC1 this loop demonstrated a strangulation movement with the backbone pointing to its own interior. This bottleneck points to the closure of output tunnel 2e. However, in PC2 the loop has acquired a range of motions for opening the connection cavity.

The greater amplitudes of movements of the FG and BC loops were observed in cytochrome P450 interacting with nicotine and NNN. Smaller amplitudes were observed in the NNK complex, so we can infer that the substrates of larger size and volume occupying the binding pocket are able to decrease the range of motion of the FG and BC loops.

3.6. Binding Free Energy and Its Components. The MM-GBSA approach was used to calculate the free energy binding of the three complexes. Considering that sufficiently large MD simulations generate many conformational configurations,⁶⁶ we selected the interval of the MD trajectory with stable conformations of the enzyme structure (regions of the RMSD plot with a plateau) to perform the binding free energy calculations. For these calculations, 500 frames of the last 5 ns of MD simulation were selected. The values obtained are shown in Figure 7.

According to our results, the interaction of nicotine, NNK, and NNN compounds with CYP2A13 is favorable with ΔG_{bind}

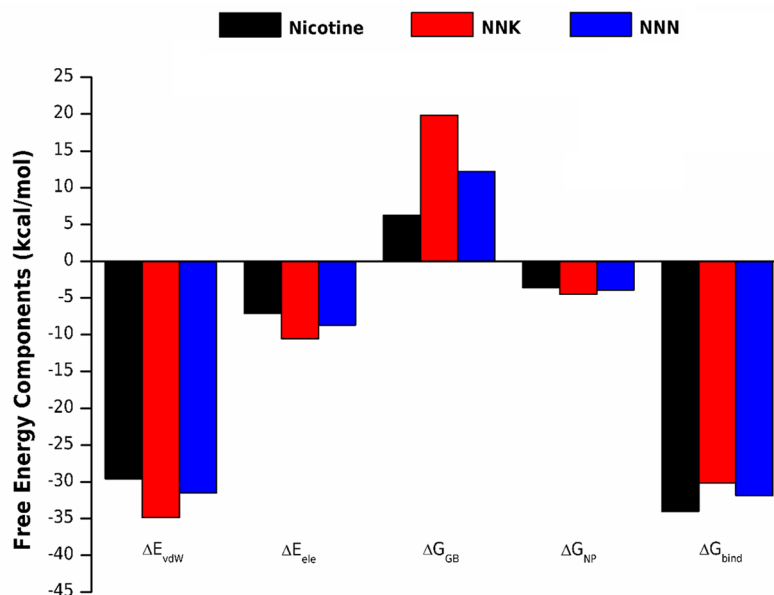


Figure 7. Binding energy values and energy components. ΔE_{vdW} , contributions by van der Waals interactions; ΔE_{ele} , electrostatic energy; ΔG_{GB} , polar solvation energy; ΔG_{NP} , nonpolar solvation energy; ΔG_{bind} , binding affinity.

being -34.06 kcal/mol, -30.16 kcal/mol, and -31.88 kcal/mol, respectively.

Together, the contributions of van der Waals interactions (ΔE_{vdW}), electrostatic energy (ΔE_{ele}), and nonpolar solvation energy (ΔG_{NP}) were favorable for the formation of the binding complex. From these values, van der Waals interactions appear to be mainly responsible for the formation of the CYP–nicotine, CYP–NNK, and CYP–NNN complexes, with the respective values being -29.58 kcal/mol, -34.86 kcal/mol, and -31.51 kcal/mol. Nonpolar contributions (ΔG_{NP}), calculated from the solvent accessible surface area (SASA), were also favorable for the formation of the complexes, although their contribution was minimal.

As expected, our results are in accordance with experimental evidence that shows the Phe cluster (Phe107, Phe111, and Phe209) creating hydrophobic interactions with NNK.¹¹ The contribution of ΔE_{vdW} for NNK is about -35 kcal/mol, followed by NNN (-32 kcal/mol) and nicotine (-30 kcal/mol). In our MD simulations, we observed important interactions of CYP2A13 with NNK, NNN, and nicotine, particularly, by the residues Phe107, Phe111, Ala117, Phe118, Phe209, Asn297, and Leu370. Binding energy analysis (Figure 7) shows that the effect of polar solvation is less destabilizing in nicotine binding than those observed in NNN and NNK. This observation may contribute to the design of attractive ligands with the potential of CYP2A13 binding. Furthermore, we evaluated the influence of CYP2A13 on the electrostatic potential surfaces of the inhibitors along the simulation and determined the molecular electrostatic potential (MEP) surfaces of the ligands (Figure S3). The MEP surfaces were obtained from the M06-2X/6-31G (d,p) level using single-point structures obtained from the MD simulations. These surfaces correspond to an isodensity value of 0.002 au. The most nucleophilic regions (negative electrostatic potential) are shown in red, whereas the most electrophilic regions (positive electrostatic potential) are shown in blue. Our results show that the electrostatic charges on nicotine may be responsible for the polar solvation energy and provide important

contributions to the design of attractive ligands with the potential of CYP2A13 binding.

CONCLUSIONS

The presence of compound I in the CYP2A13 binding site promoted changes in the binding mode of nicotine and NNK, compared to X-ray crystal structures. The crystal structures were solved in the presence of the heme group in the active site. However, the heme needed to be replaced by compound I, which hydroxylates the substrates, to investigate the conformational mechanism of the enzyme. The conformational changes were observed in the nicotine methyl pyrrolidine and the *N'*-methyl nitrosamine group of NNK. Significant conformational modifications were not visualized in the CYP2A13–NNN system because this molecule was docked in the binding pocket of the enzyme in the presence of compound I. The H-bond established between nicotine and Asn297 was essential to keeping the molecule oriented in the direction of compound I, which promotes hydroxylation at 5'- and 2'-carbons. This H-bond was formed during 91 ns of a total of 100 ns MD simulation. The PC1 vs PC2 plot revealed that cytochrome P450 interacting with nicotine, NNK, and NNN, for activation, exhibits different conformational states during the MD trajectories. When interacting with nicotine and NNK, the protein assumed more diverse conformations, whereas the conformations assumed by the NNN-bound receptor were less varied. In general, the mode of movement of the FG and BC loops was different for the three complexes. Our analyses provide relevant information for understanding the binding mode of nicotine with the cytochrome P450 2A13 isoform, the former being a highly addictive and damaging drug. We are also able to understand with more clarity, the interaction of the pro-carcinogenic agents NNK and NNN with the active cytochrome site.

■ ASSOCIATED CONTENT

Supporting Information

The Supporting Information is available free of charge on the ACS Publications website at DOI: 10.1021/acs.jcim.9b00741.

Figures S1–S3 (PDF)

■ AUTHOR INFORMATION

Corresponding Author

*Tel.: +55 91 3182-3200. E-mail: jorddynevescruz@gmail.com.

ORCID

Jorddy Neves Cruz: 0000-0003-0529-3714

Anderson Henrique Lima e Lima: 0000-0002-8451-9912

Notes

The authors declare no competing financial interest.

■ ACKNOWLEDGMENTS

J.N.C. appreciates the support of the Eliseu Alves Foundation (SAIC/Embrapa: 22500.18/0015-7). M.S.d.O. thanks Coordination for the Improvement of Higher Education Personnel (CAPES) for the doctorate scholarship (Process Number: 1.662.230). The authors acknowledge the Federal University of Para (UFPA) for providing computational resources which have contributed to the research results reported within this paper.

■ REFERENCES

- (1) Warren, G.; Singh, A. Nicotine and Lung Cancer. *J. Carcinog.* **2013**, *12*, 1.
- (2) West, R. Tobacco Smoking: Health Impact, Prevalence, Correlates and Interventions. *Psychol. Health* **2017**, *32*, 1018–1036.
- (3) WHO Report on the Global Tobacco Epidemic, Tobacco Use Kills More than 7 Million People Each Year; World Health Organization, **2017**.
- (4) Rodgman, A.; Perfetti, T.; Perfetti, T. A. *The Chemical Components of Tobacco and Tobacco Smoke*, 2nd ed.; CRC Press, **2013**; DOI: 10.1201/b13973.
- (5) Dubey, K. D.; Shaik, S. Cytochrome P450 - The Wonderful Nanomachine Revealed through Dynamic Simulations of the Catalytic Cycle. *Acc. Chem. Res.* **2019**, *52*, 389–399.
- (6) Yoshizawa, K.; Kamachi, T.; Shiota, Y. A Theoretical Study of the Dynamic Behavior of Alkane Hydroxylation by a Compound I Model of Cytochrome P450. *J. Am. Chem. Soc.* **2001**, *123*, 9806–9816.
- (7) Xue, J.; Yang, S.; Seng, S. Mechanisms of Cancer Induction by Tobacco-Specific NNK and NNN. *Cancers* **2014**, *6*, 1138–1156.
- (8) Su, T.; Bao, Z.; Zhang, Q. Y.; Smith, T. J.; Hong, J. Y.; Ding, X. Human Cytochrome P450 CYP2A13: Predominant Expression in the Respiratory Tract and Its High Efficiency Metabolic Activation of a Tobacco-Specific Carcinogen, 4-(Methylnitrosamino)-1-(3-Pyridyl)-1-Butanone. *Cancer Res.* **2000**, *60*, 5074–5079.
- (9) Jalas, J. R.; Ding, X.; Murphy, S. E. Comparative Metabolism of the Tobacco-Specific Nitrosamines 4-(Methylnitrosamino)-1-(3-Pyridyl)-1-Butanone and 4-(Methylnitrosamino)-1-(3-Pyridyl)-1-Butanol by Rat Cytochrome P450 2A3 and Human Cytochrome P450 2A13. *Drug Metab. Dispos.* **2003**, *31*, 1199–1202.
- (10) Patten, C. J.; Smith, T. J.; Murphy, S. E.; Wang, M.-H.; Lee, J.; Tynes, R. E.; Koch, P.; Yang, C. S. Kinetic Analysis of the Activation of 4-(Methylnitrosamino)-1-(3-Pyridyl)-1-Butanone by Heterologously Expressed Human P450 Enzymes and the Effect of P450-Specific Chemical Inhibitors on This Activation in Human Liver Microsomes. *Arch. Biochem. Biophys.* **1996**, *333*, 127–138.
- (11) Messina, E. S.; Tyndale, R. F.; Sellers, E. M. A Major Role for CYP2A6 in Nicotine C-Oxidation by Human Liver Microsomes. *J. Pharmacol. Exp. Ther.* **1997**, *282*, 1608–1614.
- (12) Shaik, S.; De Visser, S. P. Computational Approaches to Cytochrome P450 Function. In *Cytochrome P450: Structure, Mechanism, and Biochemistry*, 3rd ed.; Springer US, **2005**; pp 45–85, DOI: 10.1007/0-387-27447-2_2.
- (13) Hecht, S. S. Biochemistry, Biology, and Carcinogenicity of Tobacco-Specific N-Nitrosamines†. *Chem. Res. Toxicol.* **1998**, *11*, 559.
- (14) Xu, Y.; Shen, Z.; Shen, J.; Liu, G.; Li, W.; Tang, Y. Computational Insights into the Different Catalytic Activities of CYP2A13 and CYP2A6 on NNK. *J. Mol. Graphics Modell.* **2011**, *30*, 1–9.
- (15) Smith, S. G.; Goodman, J. M. Assigning the Stereochemistry of Pairs of Diastereoisomers Using GIAO NMR Shift Calculation. *J. Org. Chem.* **2009**, *74*, 4597–4607.
- (16) Chen, C. B.; Hecht, S. S.; Hoffmann, D. Metabolic Alpha-Hydroxylation of the Tobacco-Specific Carcinogen, N'-Nitrosornicotine. *Cancer Res.* **1978**, *38*, 3639–3645.
- (17) Fan, T.; Sun, G.; Zhao, L.; Cui, X.; Zhong, R. Metabolic Activation and Carcinogenesis of Tobacco-Specific Nitrosamine N'-Nitrosornicotine (NNN): A Density Function Theory and Molecular Docking Study. *Int. J. Environ. Res. Public Health* **2019**, *16*, 178.
- (18) Yuan, J.-M.; Knezevich, A. D.; Wang, R.; Gao, Y.-T.; Hecht, S. S.; Stepanov, I. Urinary Levels of the Tobacco-Specific Carcinogen N'-Nitrosornicotine and Its Glucuronide Are Strongly Associated with Esophageal Cancer Risk in Smokers. *Carcinogenesis* **2011**, *32*, 1366–1371.
- (19) Ma, G.; Yu, H.; Xu, T.; Wei, X.; Chen, J.; Lin, H.; Schüürmann, G. Computational Insight into the Activation Mechanism of Carcinogenic N'-Nitrosornicotine (NNN) Catalyzed by Cytochrome P450. *Environ. Sci. Technol.* **2018**, DOI: 10.1021/acs.est.8b02795.
- (20) Li, D.; Wang, Y.; Han, K.; Zhan, C.-G. Fundamental Reaction Pathways for Cytochrome P450-Catalyzed 5'-Hydroxylation and N-Demethylation of Nicotine. *J. Phys. Chem. B* **2010**, *114*, 9023–9030.
- (21) Lonsdale, R.; Mulholland, A. J. QM/MM Modelling of Drug-Metabolizing Enzymes. *Curr. Top. Med. Chem.* **2014**, *14*, 1339–1347.
- (22) Li, D.; Huang, X.; Han, K.; Zhan, C.-G. Catalytic Mechanism of Cytochrome P450 for 5'-Hydroxylation of Nicotine: Fundamental Reaction Pathways and Stereoselectivity. *J. Am. Chem. Soc.* **2011**, *133*, 7416–7427.
- (23) Li, D.; Huang, X.; Lin, J.; Zhan, C.-G. Catalytic Mechanism of Cytochrome P450 for N-Methylhydroxylation of Nicotine: Reaction Pathways and Regioselectivity of the Enzymatic Nicotine Oxidation. *Dalt. Trans.* **2013**, *42*, 3812.
- (24) Kwiecień, R. A.; Le Questel, J.-Y.; Lebreton, J.; Delaforge, M.; André, F.; Pihan, E.; Roussel, A.; Fournial, A.; Paneth, P.; Robins, R. J. Cytochrome P450-Catalyzed Degradation of Nicotine: Fundamental Parameters Determining Hydroxylation by Cytochrome P450 2A6 at the 5'-Carbon or the N-Methyl Carbon. *J. Phys. Chem. B* **2012**, *116*, 7827–7840.
- (25) Mittra, K.; Green, M. T. Reduction Potentials of P450 Compounds I and II: Insight into the Thermodynamics of C-H Bond Activation. *J. Am. Chem. Soc.* **2019**, *141*, 5504–5510.
- (26) Shaik, S.; Cohen, S.; Wang, Y.; Chen, H.; Kumar, D.; Thiel, W. P450 Enzymes: Their Structure, Reactivity, and Selectivity - Modeled by QM/MM Calculations. *Chem. Rev.* **2010**, *110*, 949–1017.
- (27) DeVore, N. M.; Scott, E. E. Nicotine and 4-(Methylnitrosamino)-1-(3-Pyridyl)-1-Butanone Binding and Access Channel in Human Cytochrome P450 2A6 and 2A13 Enzymes. *J. Biol. Chem.* **2012**, *287*, 26576–26585.
- (28) Salomon-Ferrer, R.; Case, D. A.; Walker, R. C. An Overview of the Amber Biomolecular Simulation Package. *Wiley Interdiscip. Rev. Comput. Mol. Sci.* **2013**, *3*, 198–210.
- (29) Neves Cruz, J.; da Costa, K. S.; de Carvalho, T. A. A.; de Alencar, N. A. N. Measuring the Structural Impact of Mutations on Cytochrome P450 21A2, the Major Steroid 21-Hydroxylase Related to Congenital Adrenal Hyperplasia. *J. Biomol. Struct. Dyn.* **2019**, *1*.
- (30) Cruz, J. N.; Costa, J. F. S.; Khayat, A. S.; Kuca, K.; Barros, C. A. L.; Neto, A. M. J. C. Molecular Dynamics Simulation and Binding

Free Energy Studies of Novel Leads Belonging to the Benzofuran Class Inhibitors of *Mycobacterium Tuberculosis* Polyketide Synthase 13. *J. Biomol. Struct. Dyn.* **2019**, *37*, 1616.

(31) Dennington, R.; Keith, T. A.; Millam, J. M. *Gauss View Version 6*; Gaussian, Inc., 2016.

(32) Frisch, M. J.; Trucks, G. W.; Schlegel, H. B.; Scuseria, G. E.; Robb, M. A.; Cheeseman, J. R.; Scalmani, G.; Barone, V.; Petersson, G. A.; Nakatsuji, H.; Li, X.; Caricato, M.; Marenich, A. V.; Bloino, J.; Janesko, B. G.; Gomperts, R.; Mennucci, B.; Hratchian, H. P.; Ortiz, J. V.; Izmaylov, A. F.; Sonnenberg, J. L.; Williams-Young, D.; Ding, F.; Lipparini, F.; Egidi, F.; Goings, J.; Peng, B.; Petrone, A.; Henderson, T.; Ranasinghe, D.; Zakrzewski, V. G.; Gao, J.; Rega, N.; Zheng, G.; Liang, W.; Hada, M.; Ehara, M.; Toyota, K.; Fukuda, R.; Hasegawa, J.; Ishida, M.; Nakajima, T.; Honda, Y.; Kitao, O.; Nakai, H.; Vreven, T.; Throssell, K.; Montgomery, J. A., Jr.; Peralta, J. E.; Ogliaro, F.; Bearpark, M. J.; Heyd, J. J.; Brothers, E. N.; Kudin, K. N.; Staroverov, V. N.; Keith, T. A.; Kobayashi, R.; Normand, J.; Raghavachari, K.; Rendell, A. P.; Burant, J. C.; Iyengar, S. S.; Tomasi, J.; Cossi, M.; Millam, J. M.; Klene, M.; Adamo, C.; Cammi, R.; Ochterski, J. W.; Martin, R. L.; Morokuma, K.; Farkas, O.; Foresman, J. B.; Fox, D. J. *Gaussian 16*, Revision B.01; Gaussian, Inc.: Wallingford, CT, 2016.

(33) Becke, A. D. Density-functional Thermochemistry. III. The Role of Exact Exchange. *J. Chem. Phys.* **1993**, *98*, 5648–5652.

(34) Lee, C.; Yang, W.; Parr, R. G. Development of the Colle-Salvetti Correlation-Energy Formula into a Functional of the Electron Density. *Phys. Rev. B: Condens. Matter Mater. Phys.* **1988**, *37*, 785–789.

(35) Thomsen, R.; Christensen, M. H. MolDock: A New Technique for High-Accuracy Molecular Docking. *J. Med. Chem.* **2006**, *49*, 3315–3321.

(36) Cuya, T.; Goncalves, A. d. S.; da Silva, J. A. V.; Ramalho, T. C.; Kuca, K.; C.C. Franca, T. The Role of the Oximes HI-6 and HS-6 inside Human Acetylcholinesterase Inhibited with Nerve Agents: A Computational Study. *J. Biomol. Struct. Dyn.* **2018**, *36*, 3444–3452.

(37) Wang, J.; Cieplak, P.; Kollman, P. A. How Well Does a Restrained Electrostatic Potential (RESP) Model Perform in Calculating Conformational Energies of Organic and Biological Molecules? *J. Comput. Chem.* **2000**, *21*, 1049–1074.

(38) Cornell, W. D.; Cieplak, P.; Bayly, C. I.; Kollman, P. A. Application of RESP Charges to Calculate Conformational Energies, Hydrogen Bond Energies, and Free Energies of Solvation. *J. Am. Chem. Soc.* **1993**, *115*, 9620–9631.

(39) Wang, J.; Wang, W.; Kollman, P. A.; Case, D. A. Automatic Atom Type and Bond Type Perception in Molecular Mechanical Calculations. *J. Mol. Graphics Modell.* **2006**, *25*, 247–260.

(40) Wang, J.; Wolf, R. M.; Caldwell, J. W.; Kollman, P. A.; Case, D. A. Development and Testing of a General Amber Force Field. *J. Comput. Chem.* **2004**, *25*, 1157–1174.

(41) Shahrokh, K.; Orendt, A.; Yost, G. S.; Cheatham, T. E. Quantum Mechanically Derived AMBER-Compatible Heme Parameters for Various States of the Cytochrome P450 Catalytic Cycle. *J. Comput. Chem.* **2012**, *33*, 119–133.

(42) Dolinsky, T. J.; Nielsen, J. E.; McCammon, J. A.; Baker, N. A. PDB2PQR: An Automated Pipeline for the Setup of Poisson-Boltzmann Electrostatics Calculations. *Nucleic Acids Res.* **2004**, *32* (Web Server), W665–W667.

(43) Maier, J. A.; Martinez, C.; Kasavajhala, K.; Wickstrom, L.; Hauser, K. E.; Simmerling, C. Ff14SB: Improving the Accuracy of Protein Side Chain and Backbone Parameters from Ff99SB. *J. Chem. Theory Comput.* **2015**, *11*, 3696–3713.

(44) Jorgensen, W. L.; Chandrasekhar, J.; Madura, J. D.; Impey, R. W.; Klein, M. L. Comparison of Simple Potential Functions for Simulating Liquid Water. *J. Chem. Phys.* **1983**, *79*, 926–935.

(45) Darden, T.; York, D.; Pedersen, L. Particle Mesh Ewald: An $N \log(N)$ Method for Ewald Sums in Large Systems. *J. Chem. Phys.* **1993**, *98*, 10089–10092.

(46) Ryckaert, J. P.; Ciccotti, G.; Berendsen, H. J. C. Numerical Integration of the Cartesian Equations of Motion of a System with

Constraints: Molecular Dynamics of n-Alkanes. *J. Comput. Phys.* **1977**, *23*, 327–341.

(47) Izaguirre, J. A.; Catarello, D. P.; Wozniak, J. M.; Skeel, R. D. Langevin Stabilization of Molecular Dynamics. *J. Chem. Phys.* **2001**, *114*, 2090–2098.

(48) Roe, D. R.; Cheatham, T. E. PTRAJ and CPPTRAJ: Software for Processing and Analysis of Molecular Dynamics Trajectory Data. *J. Chem. Theory Comput.* **2013**, *9*, 3084–3095.

(49) Amadei, A.; Linssen, A. B. M.; Berendsen, H. J. C. Essential Dynamics of Proteins. *Proteins: Struct., Funct., Genet.* **1993**, *17*, 412–425.

(50) Ichiye, T.; Karplus, M. Collective Motions in Proteins: A Covariance Analysis of Atomic Fluctuations in Molecular Dynamics and Normal Mode Simulations. *Proteins: Struct., Funct., Genet.* **1991**, *11*, 205–217.

(51) Bergonzo, C.; Henriksen, N. M.; Roe, D. R.; Swails, J. M.; Roitberg, A. E.; Cheatham, T. E. Multidimensional Replica Exchange Molecular Dynamics Yields a Converged Ensemble of an RNA Tetranucleotide. *J. Chem. Theory Comput.* **2014**, *10*, 492–499.

(52) Bakan, A.; Meireles, L. M.; Bahar, I. ProDy: Protein Dynamics Inferred from Theory and Experiments. *Bioinformatics* **2011**, *27*, 1575–1577.

(53) Bakan, A.; Dutta, A.; Mao, W.; Liu, Y.; Chennubhotla, C.; Lezon, T. R.; Bahar, I. Evol and ProDy for Bridging Protein Sequence Evolution and Structural Dynamics. *Bioinformatics* **2014**, *30*, 2681–2683.

(54) Humphrey, W.; Dalke, A.; Schulten, K. VMD: Visual Molecular Dynamics. *J. Mol. Graphics* **1996**, *14*, 33–38.

(55) Sun, H.; Li, Y.; Shen, M.; Tian, S.; Xu, L.; Pan, P.; Guan, Y.; Hou, T. Assessing the Performance of MM/PBSA and MM/GBSA Methods. 5. Improved Docking Performance Using High Solute Dielectric Constant MM/GBSA and MM/PBSA Rescoring. *Phys. Chem. Chem. Phys.* **2014**, *16*, 22035–22045.

(56) de Oliveira, M. S.; da Cruz, J. N.; Gomes Silva, S.; da Costa, W. A.; de Sousa, S. H. B.; Bezerra, F. W. F.; Teixeira, E.; da Silva, N. J. N.; de Aguiar Andrade, E. H.; de Jesus Chaves Neto, A. M.; de Carvalho, R. N. Phytochemical Profile, Antioxidant Activity, Inhibition of Acetylcholinesterase and Interaction Mechanism of the Major Components of the Piper Divaricatum Essential Oil Obtained by Supercritical CO₂. *J. Supercrit. Fluids* **2019**, *145*, 74–84.

(57) Silva, S. G.; da Costa, R. A.; de Oliveira, M. S.; da Cruz, J. N.; Figueiredo, P. L. B.; Brasil, D. do S. B.; Nascimento, L. D.; Chaves Neto, A. M. de J.; de Carvalho Junior, R. N.; Andrade, E. H. de A. Chemical Profile of Lippia Thymoides, Evaluation of the Acetylcholinesterase Inhibitory Activity of Its Essential Oil, and Molecular Docking and Molecular Dynamics Simulations. *PLoS One* **2019**, *14*, No. e0213393.

(58) Forli, S.; Huey, R.; Pique, M. E.; Sanner, M. F.; Goodsell, D. S.; Olson, A. J. Computational Protein–Ligand Docking and Virtual Drug Screening with the AutoDock Suite. *Nat. Protoc.* **2016**, *11*, 905–919.

(59) Wong, H. L.; Murphy, S. E.; Hecht, S. S. Cytochrome P450 2A-Catalyzed Metabolic Activation of Structurally Similar Carcinogenic Nitrosamines: *N'*-Nitroso-nornicotine Enantiomers, *N*-Nitrosopiperidine, and *N*-Nitrosopyrrolidine. *Chem. Res. Toxicol.* **2005**, *18*, 61–69.

(60) DeVore, N. M.; Scott, E. E. Nicotine and 4-(Methylnitrosamino)-1-(3-pyridyl)-1-Butanone Binding and Access Channel in Human Cytochrome P450 2A6 and 2A13 Enzymes. *J. Biol. Chem.* **2012**, *287*, 26576–26585.

(61) Schrödinger, L. *The PyMOL Molecular Graphics System*, version 2.2.3; Schrödinger, LLC, 2018.

(62) Schlicht, K. E.; Berg, J. Z.; Murphy, S. E. Effect of CYP2A13 Active Site Mutation N297A on Metabolism of Coumarin and Tobacco-Specific Nitrosamines. *Drug Metab. Dispos.* **2009**, *37*, 665–671.

(63) Murphy, S. E.; Raulinaitis, V.; Brown, K. M. Nicotine 5'-Oxidation and Methyl Oxidation by P450 2A Enzymes. *Drug Metab. Dispos.* **2005**, *33*, 1166–1173.

(64) Schlicht, K. E.; Berg, J. Z.; Murphy, S. E. Effect of CYP2A13 Active Site Mutation N297A on Metabolism of Coumarin and Tobacco-Specific Nitrosamines. *Drug Metab. Dispos.* **2009**, *37*, 665–671.

(65) Cojocaru, V.; Winn, P. J.; Wade, R. C. The Ins and Outs of Cytochrome P450s. *Biochim. Biophys. Acta, Gen. Subj.* **2007**, *1770*, 390–401.

(66) Gonçalves, M. A.; Santos, L. S.; Prata, D. M.; Peixoto, F. C.; da Cunha, E. F. F.; Ramalho, T. C. Optimal Wavelet Signal Compression as an Efficient Alternative to Investigate Molecular Dynamics Simulations: Application to Thermal and Solvent Effects of MRI Probes. *Theor. Chem. Acc.* **2017**, *136*, 15.